AD-A041 338 BALLISTIC RESEARCH LABS ABERDEEN PROVING GROUND MD F/G 20/4
COMPUTATIONS OF TURBULENT BOUNDARY LAYER DEVELOPMENT OVER A YAW--ETC(U)
MAY 77 W B STUREK, H A DWYER, L D KAYSER

UNCLASSIFIED BRL-1985 NL

1 OF 1
AD A041338

END

DATE FILMED
7-77

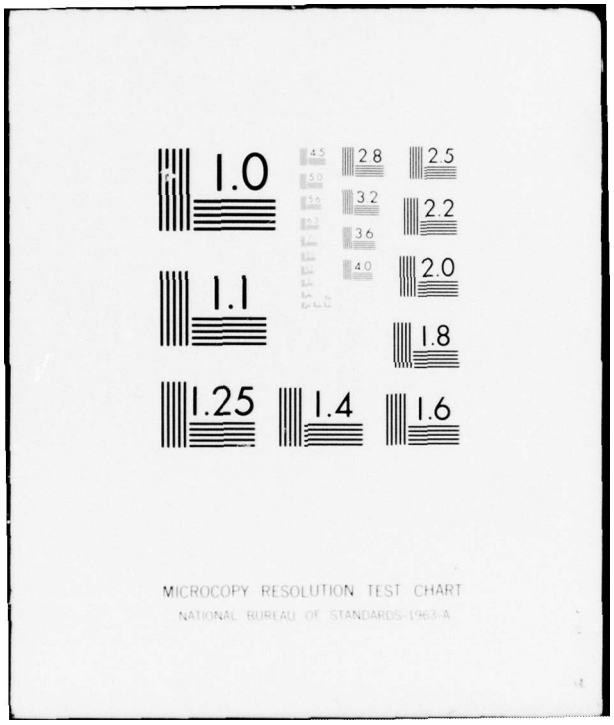
1.0
1.1
1.25
1.4
1.6
1.8
2.0
2.2
2.5
2.8
3.2
3.6
4.0
4.5
5.0
5.6
MICROCOPY RESOLUTION TEST CHART
NATIONAL BUREAU OF STANDARDS-1963-A

BRL

AD

REPORT NO. 1985

COMPUTATIONS OF TURBULENT BOUNDARY LAYER DEVELOPMENT OVER A YAWED, SPINNING BODY OF REVOLUTION WITH APPLICATION TO THE MAGNUS EFFECT

Walter B. Sturek
Harry A. Dwyer
Lyle D. Kayser
Charles J. Nietubicz
Robert P. Reklis
Klaus O. Opalka

May 1977

USA ARMAMENT RESEARCH AND DEVELOPMENT COMMAND
USA BALLISTIC RESEARCH LABORATORY
ABERDEEN PROVING GROUND, MARYLAND

Destroy this report when it is no longer needed.
Do not return it to the originator.

Secondary distribution of this report by originating or sponsoring activity is prohibited.

Additional copies of this report may be obtained from the National Technical Information Service, U.S. Department of Commerce, Springfield, Virginia 22151.

The findings in this report are not to be construed as an official Department of the Army position, unless so designated by other authorized documents.

UNCLASSIFIED

SECURITY CLASSIFICATION OF THIS PAGE (When Data Entered)

REPORT DOCUMENTATION PAGE		READ INSTRUCTIONS BEFORE COMPLETING FORM
1. REPORT NUMBER BRL Report No. 1985	2. GOVT ACCESSION NO.	3. RECIPIENT'S CATALOG NUMBER
4. TITLE (and Subtitle) COMPUTATIONS OF TURBULENT BOUNDARY LAYER DEVELOPMENT OVER A YAWED, SPINNING BODY OF REVOLUTION WITH APPLICATION TO THE MAGNUS EFFECT.		5. TYPE OF REPORT & PERIOD COVERED Final rept., 6. PERFORMING ORG. REPORT NUMBER
7. AUTHOR(s) Walter B. Sturek, Harry A. Dwyer, Lyle D. Kayser, Charles J. Nietubicz, Robert P. Reklis, and Klaus O. Opalka		8. CONTRACT OR GRANT NUMBER(s)
9. PERFORMING ORGANIZATION NAME AND ADDRESS U.S. Army Ballistic Research Laboratory Aberdeen Proving Ground, Maryland 21005		10. PROGRAM ELEMENT, PROJECT, TASK AREA & WORK UNIT NUMBERS RDT&E 1L161102AH43
11. CONTROLLING OFFICE NAME AND ADDRESS US Army Materiel Development & Readiness Command 5001 Eisenhower Avenue Alexandria, Virginia 22333		12. REPORT DATE MAY 1977 13. NUMBER OF PAGES 35
14. MONITORING AGENCY NAME & ADDRESS (if different from Controlling Office)		15. SECURITY CLASS. (of this report) Unclassified 15a. DECLASSIFICATION/DOWNGRADING SCHEDULE

16. DISTRIBUTION STATEMENT (of this Report)

Approved for public release; distribution unlimited.

17. DISTRIBUTION STATEMENT (of the abstract entered in Block 20, if different from Report)

18. SUPPLEMENTARY NOTES

19. KEY WORDS (Continue on reverse side if necessary and identify by block number)

Three Dimensional Boundary Layer
Turbulent Boundary Layer
Body of Revolution
Magnus Effects
Aerodynamic Coefficients

20. ABSTRACT (Continue on reverse side if necessary and identify by block number)

(1cb)
Many projectiles used by the Army are slender bodies of revolution which are launched at high spin rates. Magnus forces and moments are generated by the distorted boundary layer which results from a spinning body at angle of yaw. The Ballistic Research Laboratory is conducting and supporting theoretical and experimental Magnus research efforts. The theoretical effort involves: (1) numerical calculation of the fully three-dimensional boundary layer with the added complication of interaction between surface spin and cross flow
(Continued)

DD FORM 1 JAN 73 1473 EDITION OF 1 NOV 65 IS OBSOLETE

UNCLASSIFIED

SECURITY CLASSIFICATION OF THIS PAGE (When Data Entered)

050 750

20. ABSTRACT (Continued):

velocity; (2) three-dimensional inviscid flow calculations over a body plus boundary layer displacement surface with no plane of symmetry. Several types of experimental data, such as surface pressures, Magnus forces, boundary layer surveys, flow visualization, and skin friction, were obtained to evaluate and provide guidance to the theoretical effort. Comparison of the theory to experimental data shows the agreement to be very good.

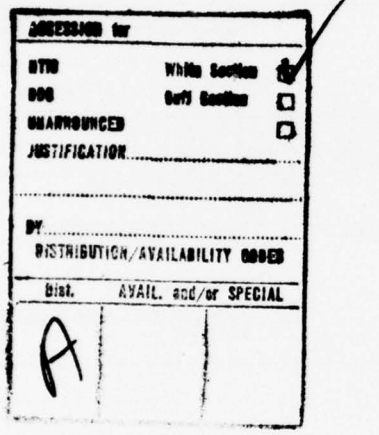

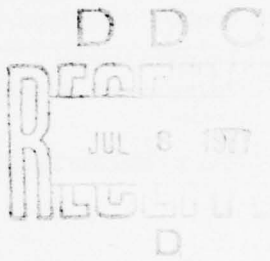

TABLE OF CONTENTS

		Page
	LIST OF ILLUSTRATIONS	5
I.	INTRODUCTION	7
II.	THEORETICAL APPROACH	7
	A. Background	7
	B. Boundary Layer Computations	8
	C. Three Dimensional Displacement Surface	10
	D. Inviscid Computations	11
	E. Sequence of Computations	11
	F. Boundary Layer Components of Magnus	12
III.	EXPERIMENTS	13
	A. General	13
	B. Boundary Layer Measurements	13
	C. Force Measurements	14
IV.	DISCUSSION OF THE THEORETICAL AND EXPERIMENTAL RESULTS	14
	A. Boundary Layer Characteristics, $\alpha < 4.2$ degrees	14
	B. Boundary Layer Characteristics, $\alpha > 4.2$ degrees	16
	C. Magnus Characteristics	16
V.	CONCLUDING REMARKS	17
	REFERENCES	18
	LIST OF SYMBOLS	31
	DISTRIBUTION LIST	33

LIST OF ILLUSTRATIONS

Figure		Page
1.	Magnus and Normal Forces on a Spinning Projectile	19
2.	Schematic Illustration of Spin Induced Boundary Layer Distortion	19
3.	Coordinate System	20
4.	Computations of δ^*_{3D} for the SOC Model, ω = 30,000 RPM	20
5.	Sequence of Numerical Computations	21
6.	Surface Pressure Distribution on the SOC Model	22
7.	Turbulent Boundary Layer Contributions to Magnus Force	22
8.	Velocity Profiles, Theory Compared With Experiment	23
9.	Velocity Profiles, Theory Compared With Experiment	23
10.	Experimental Velocity Profiles, Effects of Spin	24
11.	Boundary Layer Displacement Thickness, δ^*_x, Compared With Experiment, SOC Model	25
12.	Increment of Displacement Thickness, $\Delta\delta^*_x$, Due to Spin, SOC Model	26
13.	Preston Tube Skin Friction Results, SOC Model	27
14.	Vapor Screen Photograph, SOC Model, M = 3.0, $\alpha = 10°$	28
15.	Experimental Velocity Profiles, Effects of Spin, $\alpha = 6.3°$	29
16.	Experimental Boundary Layer Displacement Thickness, SOC Model, $\alpha = 6.3°$	29
17.	Magnus Force Vs Angle of Attack, Theory Compared With Experiment	30

I. INTRODUCTION

Many projectiles used by the Army are slender bodies of revolution which are launched at high spin rates. Magnus forces and moments are generated by the distorted boundary layer which results from a spinning body at angle of yaw. Recent Army interest in achieving increased range and greater payload capacity in artillery projectiles has led to designs with long, slender ogives, increased projectile length, and boattailed afterbodies. These designs have resulted in decreased drag with a resulting increase in range; however, the aerodynamic stability of these shapes is less than more conventional designs. This means that these new shapes are more susceptible to a Magnus induced instability. The Magnus force is small (Figure 1), typically 1/10 to 1/100 of the normal force; however, its effect is important because the Magnus moment acts to undamp the projectile throughout its flight. Thus, it is desirable to minimize the Magnus moment in order for the projectile to fly at a small average angle of attack and achieve the greatest range capability.

Magnus has been modeled theoretically as resulting from spin induced distortion of the boundary layer. This effect is illustrated schematically in Figure 2 where a cross-sectional view of a body of revolution is shown. The body is at angle of attack as indicated by the cross flow velocity. In the view where there is no surface spin, the profile of the edge of the boundary layer is symmetric with respect to the plane of the angle of attack. In the view where the surface is spinning, the profile of the boundary layer is asymmetric with respect to the plane of the angle of attack--thus, the inviscid pressure distribution (which responds to the aerodynamic shape composed of the model + boundary-layer-displacement-surface) is asymmetric and yields a net side force.

The U.S. Army Ballistic Research Laboratory has placed increased emphasis on research into the Magnus effect. In this paper, recent results of an effort to develop a method for computing Magnus effects for use in projectile design will be discussed and results of related experimental studies will be presented.

II. THEORETICAL APPROACH

A. Background

Since the Magnus effect is a viscous phenomena, computation of the boundary layer development is the foundation for computations of the Magnus force. The boundary layer we are considering is fully three dimensional with the added complication of the interaction of surface spin with the cross flow velocity. The inviscid flow also requires special attention since, in order to compute the Magnus force, the inviscid flow computation technique must be able to compute the three-

dimensional flow over a body + boundary-layer-displacement-surface with no plane of symmetry.

B. Boundary Layer Computations

The basic equations defining the three dimensional compressible, turbulent boundary layer flow over an axisymmetric body of revolution described by the relation $r = r(x)$ are listed below. The coordinate system is shown in Figure 3.

Continuity

$$\frac{\partial}{\partial x}(r\bar{\rho}\bar{u}) + \frac{\partial}{\partial y}(r\bar{\rho}\hat{v}) + \frac{\partial}{\partial \phi}(\bar{\rho}\bar{w}) = 0 \tag{1}$$

x-Momentum

$$\bar{\rho}\left[\bar{u}\frac{\partial \bar{u}}{\partial x} + \hat{v}\frac{\partial \bar{u}}{\partial y} + \frac{\bar{w}}{r}\frac{\partial \bar{u}}{\partial \phi} - \frac{\bar{w}^2}{r}\frac{\partial r}{\partial x}\right] = -\frac{\partial \bar{p}_e}{\partial x} + \frac{\partial}{\partial y}\left[\mu\frac{\partial \bar{u}}{\partial y} - \overline{\rho u'v'}\right] \tag{2}$$

ϕ-Momentum

$$\bar{\rho}\left[\bar{u}\frac{\partial \bar{w}}{\partial x} + \hat{v}\frac{\partial \bar{w}}{\partial y} + \frac{\bar{w}}{r}\frac{\partial \bar{w}}{\partial \phi} + \frac{\bar{u}\bar{w}}{r}\frac{\partial r}{\partial x}\right] = -\frac{1}{r}\frac{\partial \bar{p}_e}{\partial \phi} + \frac{\partial}{\partial y}\left[\mu\frac{\partial \bar{w}}{\partial y} - \overline{\rho v'w'}\right] \tag{3}$$

Energy

$$\begin{aligned}\bar{\rho}\left[\bar{u}\frac{\partial \bar{h}}{\partial x} + \hat{v}\frac{\partial \bar{h}}{\partial y} + \frac{\bar{w}}{r}\frac{\partial \bar{h}}{\partial \phi}\right] &= \bar{u}\frac{\partial \bar{p}_e}{\partial x} + \frac{\bar{w}}{r}\frac{\partial \bar{p}_e}{\partial \phi} + \mu\left[\left(\frac{\partial \bar{u}}{\partial y}\right)^2 + \left(\frac{\partial \bar{w}}{\partial y}\right)^2\right] \\ &\quad - \overline{\rho u'v'}\frac{\partial \bar{u}}{\partial y} - \overline{\rho v'w'}\frac{\partial \bar{w}}{\partial y} + \frac{\partial}{\partial y}\left[\frac{\mu}{Pr}\frac{\partial \bar{h}}{\partial y} - \overline{\rho v'h'}\right].\end{aligned} \tag{4}$$

where $\hat{v} = \bar{v} + \dfrac{\overline{\rho' v'}}{\bar{\rho}}$ and the bar indicates a time averaged quantity.

In order to obtain closure for this system of equations, the following models of the turbulence terms have been introduced:

Turbulent Shear Stress

$$-\overline{\rho u'v'} = -\overline{\rho v'w'} = \bar{\rho}\,\ell^2\left[\left(\frac{\partial \bar{u}}{\partial y}\right)^2 + \left(\frac{\partial \bar{w}}{\partial y}\right)^2\right] = \varepsilon\left[\left(\frac{\partial \bar{u}}{\partial y}\right)^2 + \left(\frac{\partial \bar{w}}{\partial y}\right)^2\right]^{1/2}$$

where ε is introduced as the turbulent eddy viscosity and the mixing length, $\ell = .09\,\delta \tanh[(.4/.09)(y/\delta)]$. Van Driest damping is used to account for the effect of the laminar sublayer.

Turbulent Heat Transfer

$$- \overline{\rho v'' h''} = \frac{k_t}{c_p} \frac{\partial \bar{h}}{\partial y}$$

The turbulent Prandtl number is introduced as

$$Pr_t = c_p \varepsilon / k_t = 0.90$$

The numerical technique used to solve these equations is an implicit technique developed by Dwyer[1,2] that takes into consideration the changes in direction of the cross flow velocity that occurs on the side of the model where the inviscid cross flow opposes surface spin. This technique correctly models the cross flow convection process occurring within the boundary layer. In order to improve the speed and accuracy of the numerical solution, several coordinate transformations are employed:

Mangler transformation of axisymmetric growth,

$$\xi = \int_o^x r^2 \, dx \quad ;$$

Blasius type transformation of normal growth,

$$\eta = \frac{p_\infty}{p_e}^{\frac{1}{2}} \frac{\rho_\infty u_\infty}{2 \mu_\infty \xi}^{\frac{1}{2}} \int_o^y \frac{\rho}{\rho_\infty} \, r \, dy \quad ; \quad \text{and}$$

coordinate stretching to allow closer grid spacing near the wall[3],

$$n_j = 100 \, (1.5 \exp [(j-1)(1/60)(1/.05)] - 1)/(1.5 \exp (1/.05) - 1)$$

where j = 1, 2, 3, ... 61

---

1. *H. A. Dwyer, "Three Dimensional Flow Studies Over a Spinning Cone at Angle of Attack," BRL Contract Report No. 137, February 1974, U.S. Army Ballistic Research Laboratories, Aberdeen Proving Ground, Maryland. AD 774795.*
2. *H. A. Dwyer and B. R. Sanders, "Magnus Forces on Spinning Supersonic Cones. Part I: The Boundary Layer," BRL Contract Report No. 248, July 1975, U.S. Army Ballistic Research Laboratories, Aberdeen Proving Ground, Maryland. AD A013518. Also AIAA Journal, Vol. 14, No. 4, April 1976, p. 498.*
3. *F. G. Blottner, "Variable Grid Scheme Applied to Turbulent Boundary Layers," Journal of Computer Methods in Applied Mechanics and Engineering, 1975.*

In computing the boundary layer development, the effect of turbulence is turned on gradually over three longitudinal steps. The computation grid in the azimuthal plane is in 10 degree increments. Three iterations are performed at each station for turbulent computations. For comparison with experiment, the location of boundary layer transition is fixed at the location of the boundary layer trip on the experimental model.

C. Three Dimensional Displacement Surface

The three dimensional displacement surface is not merely the vector sum of the longitudinal and circumferential components of the boundary-layer displacement thicknesses. Instead, the differential equation derived by Moore[4]:

$$\frac{\partial}{\partial x}\left[\rho_e u_e r\left(\delta^*_{3D} - \delta^*_x\right)\right] + \frac{\partial}{\partial \phi}\left[\rho_e w_e\left(\delta^*_{3D} - \delta^*_\phi\right)\right] = 0 \tag{5}$$

must be solved for δ^*_{3D}, the three dimensional boundary-layer displacement thickness where

$$\delta^*_x = \int_0^\delta \left(1 - \frac{\rho u}{\rho_e u_e}\right) dy \quad \text{and} \quad \delta^*_\phi = \int_0^\delta \left(1 - \frac{\rho w}{\rho_e w_e}\right) dy$$

Dwyer[5] has shown that equation (5) is of the general form

$$P\frac{\partial \delta^*_{3D}}{\partial x} + Q\frac{\partial \delta^*_{3D}}{\partial \phi} = R_1 \delta^*_{3D} + R_2 \tag{6}$$

The singularity in δ^*_{3D} and δ^*_x at $x = 0$ can be avoided by starting the computations at a small, finite value of x and computing approximate starting conditions. Equation (6) can then be solved as an ordinary differential equation, providing the differencing in the circumferential direction is carried out from $\phi = 0$ to 180° and from $\phi = 0$ to -180° in order to obey the zone of influence defined by

---

4. *F. N. Moore, "Displacement Effect of a Three-Dimensional Boundary Layer," NACA TN 2722, June 1952.*

5. *H. A. Dwyer, "Methods for Computing Magnus Effects on Artillery Projectiles," BRL Contract Report No. 329, January 1977, U.S. Army Ballistic Research Laboratory, Aberdeen Proving Ground, Maryland. AD A035330.*

$$\frac{dx}{d\phi} = r \frac{u_e}{w_e} .$$

An example of computed values of δ^*_{3D} for the SOC model is shown in Figure 4. The effect of spin is to decrease the thickness of the boundary layer where surface spin and inviscid crossflow are in the same direction and to increase the thickness of the boundary layer where surface spin and inviscid crossflow oppose.

D. Inviscid Computations

The development of a numerical technique for computing the three dimensional inviscid flow field over a yawed, pointed, body in supersonic flow was a very important step in the development of a capability for computing Magnus effects[6]. The program uses MacCormack's[7] "shock capturing" numerical technique. This is a second order accurate scheme that uses a predictor-corrector technique to solve the equations of motion in an implicit marching scheme. The unique feature of the program developed by Sanders for the Magnus problem is that the flow field is computed about an axisymmetric model plus displacement surface which, due to the distortion of the boundary layer by surface spin, has no plane of symmetry.

E. Sequence of Computations

The sequence of computations which must be run in order to compute Magnus effects is indicated in Figure 5. Each block indicates a separate computer program along with its required input information and the output. The two main programs are outlined in asterisks.

In order to start the computations, an initial plane of profile data at the tip of the model and inviscid flow boundary conditions are required. The initial profile data are computed for the limiting condition of the conical tip of the model. The inviscid flow boundary conditions are computed using the program developed by Sanders[6]. An example showing the computed wall pressure distribution compared to experimental data for several azimuthal stations is shown in Figure 6. Also shown is the outline of the model shape, a six

---

6. *B. R. Sanders, "Three-Dimensional, Steady, Inviscid Flow Field Calculations With Application to the Magnus Problem," PhD Dissertation, University of California, Davis, California, May 1974.*

7. *R. W. MacCormack, "Numerical Solution of the Interaction of a Shock Wave With a Laminar Boundary Layer," Proceedings of the International Conference on Numerical Methods in Fluid Dynamics, Lecture Notes in Physics, Vol. 8, Maurice Holt, ed., Springer-Verlag, 1971.*

caliber long secant-ogive-cylinder. As seen in the figure, excellent agreement is obtained between theory and experiment for the moderate angle of attack considered here. It is seen that the boundary layer experiences a significant history of favorable and adverse pressure gradients in both the longitudinal and circumferential directions.

In order to start the boundary layer computation for the spinning model, initial profile data are generated for the limiting case of the laminar boundary layer at the tip of a non-spinning cone. These data, along with the outer boundary condition of the inviscid flow, enable the marching technique to begin for specific conditions of Mach number, angle of attack, wall temperature, spin rate, and free stream properties. The output of the boundary layer program consists of wall shear and centrifugal pressure gradient contributions to the Magnus effect and the longitudinal and circumferential components of the boundary layer displacement surface as functions of longitudinal and circumferential position over the entire surface of the model.

The output of the boundary layer program is input to the program which solves for the three dimensional boundary layer displacement thickness, δ^*_{3D}. Input data for this program are in the surface coordinate system used for the boundary layer computations. The output of this program is transformed into a cylindrical coordinate system in order to facilitate computation of the inviscid flow. The output consists of the surface coordinates of the model plus δ^*_{3D} as well as the local derivatives of the surface coordinate plus δ^*_{3D} in the axial and circumferential directions.

The final step is the computation of the inviscid flow over the newly defined body which is of completely arbitrary configuration with no plane of symmetry. The starting conditions consist of the inviscid flow field for the asymptotic cone tip of the original model. Pitch and yaw plane force and moment aerodynamic coefficients are the final outputs obtained.

F. Boundary Layer Components of Magnus

Due to spin induced asymmetry in the computed velocity profiles, three contributions to the Magnus effect are generated within and at the surface of the spinning model which are in addition to the boundary layer displacement effect sensed by the outer inviscid flow. These components are: (1) longitudinal velocity wall shear, $\tau_x = \mu \, (\partial u/\partial y)_{y=0}$; (2) circumferential velocity wall shear, $\tau_\phi = \mu \, (\partial w/\partial y)_{y=0}$; and (3) centrifugal pressure gradient, $\Delta p = \int_0^y \rho \, \frac{w^2}{r} \, dy$. For a non-spinning model, the net contribution of each of these components would be zero.

However, due to the asymmetry induced by surface spin, a small contribution to a side force is obtained. The relative magnitudes of these components of the Magnus force are shown in Figure 7.

III. EXPERIMENTS

A. General

The purpose of the experimental studies is to provide data that will be useful in evaluating and providing guidance for the development of the theoretical effort. The experimental studies consisted of: (1) boundary layer profile measurements; (2) optical studies; (3) Preston tube skin friction measurements; (4) strain-gage balance force measurements; and (5) wall static pressure measurements.

Experimental results were obtained in the BRL Supersonic Wind Tunnel No. 1 which is a continuous flow, flexible nozzle tunnel capable of Mach numbers 1.5 to 5.0; the test section size is 38 cm high by 33 cm wide. Data were obtained at Mach 3.0, a Reynolds number (Re_ℓ) of 7.6×10^6 and at both spinning and non-spinning conditions.

The model tested was the six caliber secant-ogive-cylinder with geometry as shown in the pressure distribution plot of Figure 6. The model was equipped with a boundary layer trip located 0.7 caliber from the nose to insure a consistent turbulent flow for all tests.

B. Boundary Layer Measurements

Measurements of the total head pressure through the boundary layer were made with a flattened impact pressure probe 0.15 cm wide by 0.015 cm high. Data were obtained on the cylindrical section at 3.33, 4.44, and 5.56 calibers from the nose and azimuthally around the model in 30 degree increments and at yaw angles from 0 to 6.3 degrees. At each position, surveys were made at both zero RPM and 20,000 RPM; the spin rate of 20,000 RPM corresponds to a pd/V of 0.19. The impact pressure probe was brought from outside the boundary layer down to, and contacting, the model surface for the zero RPM case; for the 20,000 RPM spin rate the probe was brought down to within approximately 0.01 cm from the surface. The probe axis was aligned longitudinally with the model axis. Some uncertainty is inherent in the profile data due to the probe not being aligned with the local flow direction within the boundary layer. This uncertainty would be greatest near the surface of the model and at longitudinal stations near the forward portion of the model. However, the large gradients present in a turbulent boundary layer would confine the greatest effect of flow angularity to a very small region near the surface which cannot be probed accurately using a total head probe. Also, these measurements were obtained at small angles of attack. Local Mach numbers within the boundary layer were deter-

mined from the Rayleigh pitot formula assuming a constant static pressure through the boundary layer. The boundary layer data for this paper uses measured values of wall static pressure.

Wall shear stress was obtained for the non-spinning model using the Preston tube technique. The Preston tube is a circular, total-head probe mounted flush with the model surface and sized to lie within the logarithmic portion of the law-of-the-wall velocity profile. The wall shear stress was computed from the measured impact and surface pressures and using the correlation relations of reference 8.

Vapor screen flow visualization experiments using the technique described in reference 9 were performed. The purpose of this phase was to obtain a better understanding of the surrounding flow field and in particular determine the presence of vortices both imbedded in the boundary layer and separated from the model surface. Vapor screen pictures were obtained at each ½ caliber position for angles of yaw of 2, 4, 5, 6, and 10 degrees both with and without spin.

C. Force Measurements

Measurements of Magnus and normal force were obtained using the strain-gage balance technique. The model is free to rotate on internally mounted bearings and equipped with a single row of turbine blades so that spin-up can be achieved. Turbine air is supplied to the model through the sting and the model is brought up to speeds as high as 40,000 RPM. The turbine air is then cut off and data are acquired as the model spin rate decays.

IV. DISCUSSION OF THE THEORETICAL AND EXPERIMENTAL RESULTS

A. Boundary Layer Characteristics, $\alpha < 4.2$ degrees

A comparison of theoretical and experimental velocity profiles is shown in Figure 8 for 2 degrees angle of attack and zero spin rate. The agreement is considered to be good and is actually comparable to that obtained for supersonic two-dimensional flow measurements. On the

---

8. *P. Bradshaw and K. Unsworth, "A Note on Preston Tube Calibrations in Compressible Flow," IC Aero Report 73-07, September 1973, Imperial College of Science and Technology, London, Great Britain.*

9. *C. J. Nietubicz, "Vapor Screen Technique Development at the Ballistic Research Laboratories," BRL Memorandum Report No. 2387, June 1974, U.S. Army Ballistic Research Laboratories, Aberdeen Proving Ground, Maryland. AD 784077.*

leeward side, near $\phi = 180°$, the theoretical velocities are greater than the experimental measurements near the surface and the theoretical velocities are smaller than the experimental velocities near the edge of the boundary layer. On the windward side, near $\phi = 0°$, the situation is reversed. These differences in profile shape will give compensating effects when computing integral parameters. Figure 9 compares theoretical and experimental velocity profiles at 4.2 degrees angle of attack. The differences between theoretical and experimental profile shape are similar to those at $\alpha = 2°$ except that they are more pronounced; also, the variation in boundary layer thickness from the windward to the leeward side is greater for the 4.2° case.

The effect of spin on velocity profiles is shown in Figure 10 where profiles on the side where cross flow and spin are in the same direction (ϕ = 0-180) are compared with profiles on the opposite side of the model (ϕ = 180-360) where the cross flow is in the opposite direction of spin. On the windward side of the model (ϕ = 0-90), there is almost no measurable effect of spin. On the leeward side (ϕ = 120 vs 240 and 150 vs 210), the profile shapes differ substantially. The effect of cross flow in opposition to model surface rotation (e.g. ϕ = 210) is to decrease the fullness of the profile which, of course, will result in a larger displacement thickness. It is of interest to note that the primary effect of spin is to change the profile shape rather than to change the total thickness.

Values for the longitudinal component of displacement thickness are compared in Figure 11. The agreement between theory and experiment is generally good; however, it is seen at the forward station (Z/D = 3.33) that theoretical thicknesses are slightly greater than experiment ($\phi \approx 0$) and at the aft station theoretical thicknesses are slightly smaller than experiment. This situation indicates that the boundary layer actually grows at a faster rate than predicted by theory; however, this is not particularly surprising since the turbulence model did not provide for any adjustment as a function of pressure gradient. The effect of spin on displacement thickness δ^*_x can be seen in Figure 12 where the increment of δ^*_x due to spin is plotted on an expanded scale for $\alpha = 4.2$ degrees. The effect on displacement thickness is seen to be significant only in the vicinity of the leeward side ($\phi = 180°$). The agreement between theory and experiment is encouraging evidence that the numerical technique accurately models the effect of surface spin.

Measured values for skin friction coefficient obtained using the Preston tube technique are compared to theory in Figure 13. The skin friction coefficient is referenced to free stream static properties upstream of the model rather than the more conventional approach of using local properties at the edge of the boundary layer. The agreement indicated is within ± 10%. This is considered quite good since the Preston tube is expected to yield an accuracy of ± 10% for two

dimensional flat plate boundary layer flow. The use of the Preston tube to obtain measurements in a three dimensional boundary layer flow using two dimensional calibration data must be regarded as speculative and mainly of qualitative interest.

B. Boundary Layer Characteristics, $\alpha > 4.2$ degrees

No boundary layer calculations have been made for angles of attack greater than 4.3 degrees. Experimental data at larger angles of attack shown in Figures 14, 15, and 16 illustrate difficulties that may be encountered in theoretical calculations. A representative sample of the vapor screen data is shown in Figure 14 for $\alpha = 10°$. The vapor screen is positioned 5.5 calibers behind the nose and normal to the model axis of symmetry. A symmetrical pair of separated body vortices are visible as dark regions on the leeward side. Data obtained at 6.3 degrees show the vortices to be formed but they are embedded within the boundary layer. Although the present interest is at lower angles of attack, Figure 14 is presented here for clarity purposes.

Velocity profiles at $\alpha = 6.34°$ are shown in Figure 15. On the windward side of the model, the profiles seem well behaved; however, on the leeward side (ϕ = 120-240), profiles differ drastically with each other. For example, at $\phi = 180°$ the profile shows a fullness typical of profiles seen in a favorable pressure gradient; at $\phi = 210°$, the profile is less full and seems to be tending toward separation, typical of profiles in an adverse pressure gradient. The displacement thickness at $\phi = 210°$ is actually greater than that at $\phi = 180°$ even though the total thickness is smaller than that at $\phi = 180°$. Another characteristic, which at first appears abnormal, is the large difference in boundary layer thicknesses at ϕ = 210 and 240 degrees. Displacement thicknesses at $\alpha = 6.34°$ are shown in Figure 16. The significant difference from the 4.2° case is the dip or decrease in δ^* near $\phi = 180°$. It is believed that the above phenomena are caused by the existence of longitudinal separation type vortices which are beginning to develop. Such vortices could create local areas of favorable and adverse pressure gradients that would cause the complex flows illustrated by Figures 15 and 16.

C. Magnus Characteristics

One criterion which can be used to gage the success of the theory is the accuracy with which Magnus forces and moments can be predicted. Figure 17 is a comparison of theoretical and experimental Magnus forces; in addition, the magnitude of the four components of the Magnus force are shown. The contributions of τ_ϕ and Δp oppose and are of comparable magnitude, while the contribution of τ_x is minimal. The arithmetic sum of the three boundary layer components is indicated by $C_{YBL} = \tau_x + \tau_\phi + \Delta p$. The total computed Magnus force shown here is the

arithmetic sum of the contributions due to τ_x, τ_ϕ, Δp, and δ^*_{3D}. It is worthwhile to emphasize that this marks the first time that computations of the Magnus effect have been carried out in a conceptually "exact" manner for the turbulent boundary layer on a realistic projectile configuration. The agreement between the calculated Magnus force and experimental strain-gage balance force measurements is extremely good. The theoretical computations accurately reproduce the nonlinear trend of Magnus with angle of attack. This nonlinear behavior is due primarily to the increasing dominance of the contribution of δ^*_{3D} as the angle of attack increases.

V. CONCLUDING REMARKS

A combined theoretical-experimental study of the Magnus effect on yawed, spinning projectiles has been discussed. The overall objective of this effort is to develop a method for computing Magnus effects that could be used in the design of artillery projectiles. Numerical techniques have been developed for computing: (1) the three-dimensional turbulent boundary layer development over a yawed, spinning body of revolution; (2) the three-dimensional boundary-layer displacement surface for an arbitrary body of revolution; and (3) the three-dimensional inviscid flow field over a yawed, pointed body of completely general configuration with no plane of symmetry. The computations have been compared to experimental measurements of Magnus force and turbulent boundary layer profile characteristics. The general impression obtained in comparing the computations to experimental data is that the numerical techniques are working quite well and yielding very impressive agreement with experimental data. The results for Magnus force are considered extremely encouraging. The comparisons with detailed profile characteristics do reveal minor differences. It is believed that additional accuracy can be achieved by improved or more complex turbulence modeling which accounts for both favorable and adverse pressure gradients. Other refinements in the boundary layer computation such as correction for transverse curvature and inclusion of boundary region effects should be incorporated.

The ability to predict the point of transition may be a factor in the accuracy of the theoretical model. The location of transition was fixed by the use of boundary layer trips for all the experiments described; therefore, the theoretical results do not reflect any error which might be caused in predicting the location of the transition line around the model.

The higher angle of attack experiments suggest that problems will be encountered in extending the theory to angles of attack greater than 5 degrees.

REFERENCES

1. H. A. Dwyer, "Three Dimensional Flow Studies Over a Spinning Cone at Angle of Attack," BRL Contract Report No. 137, February 1974, U.S. Army Ballistic Research Laboratories, Aberdeen Proving Ground, Maryland. AD 774795.

2. H. A. Dwyer and B. R. Sanders, "Magnus Forces on Spinning Supersonic Cones. Part I: The Boundary Layer," BRL Contract Report No. 248, July 1975, U.S. Army Ballistic Research Laboratories, Aberdeen Proving Ground, Maryland. AD A013518. Also *AIAA Journal*, Vol. 14, No. 4, April 1976, p. 498.

3. F. G. Blottner, "Variable Grid Scheme Applied to Turbulent Boundary Layers," *Journal of Computer Methods in Applied Mechanics and Engineering*, 1975.

4. F. N. Moore, "Displacement Effect of a Three-Dimensional Boundary Layer," NACA TN 2722, June 1952.

5. H. A. Dwyer, "Methods for Computing Magnus Effects on Artillery Projectiles," BRL Contract Report No. 329, January 1977, U.S. Army Ballistic Research Laboratory, Aberdeen Proving Ground, Maryland. AD A035330.

6. B. R. Sanders, "Three-Dimensional, Steady, Inviscid Flow Field Calculations With Application to the Magnus Problem," PhD Dissertation, University of California, Davis, California, May 1974.

7. R. W. MacCormack, "Numerical Solution of the Interaction of a Shock Wave With a Laminar Boundary Layer," *Proceedings of the International Conference on Numerical Methods in Fluid Dynamics*, *Lecture Notes in Physics*, Vol. 8, Maurice Holt, ed., Springer-Verlag, 1971.

8. P. Bradshaw and K. Unsworth, "A Note on Preston Tube Calibrations in Compressible Flow," IC Aero Report 73-07, September 1973, Imperial College of Science and Technology, London, Great Britain.

9. C. J. Nietubicz, "Vapor Screen Technique Development at the Ballistic Research Laboratories," BRL Memorandum Report No. 2387, June 1974, U.S. Army Ballistic Research Laboratories, Aberdeen Proving Ground, Maryland. AD 784077.

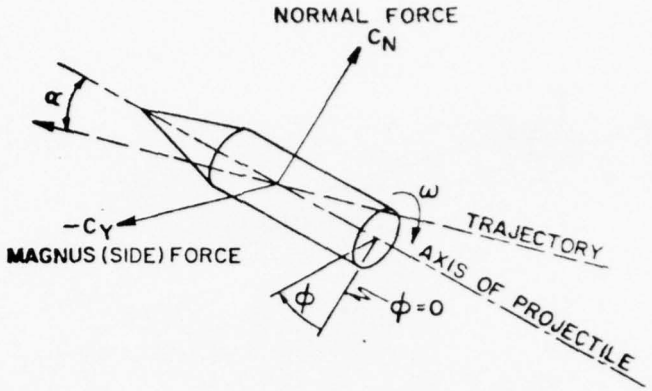

Figure 1. Magnus and Normal Forces on a Spinning Projectile

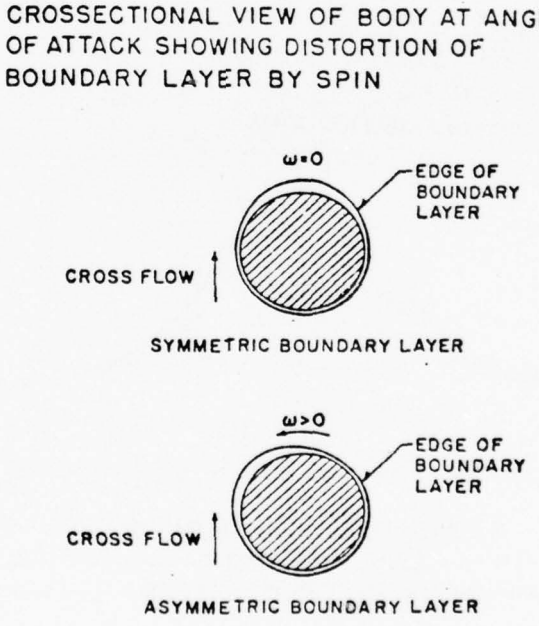

Figure 2. Schematic Illustration of Spin Induced Boundary Layer Distortion

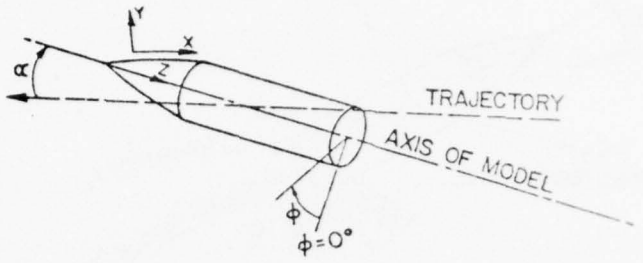

Figure 3. Coordinate System

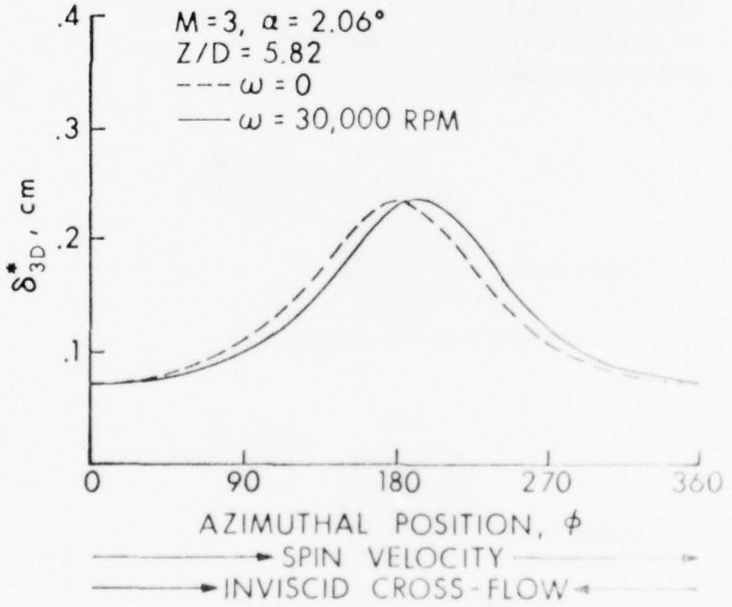

Figure 4. Computations of δ^*_{3D} for the SOC Model, ω = 30,000 RPM

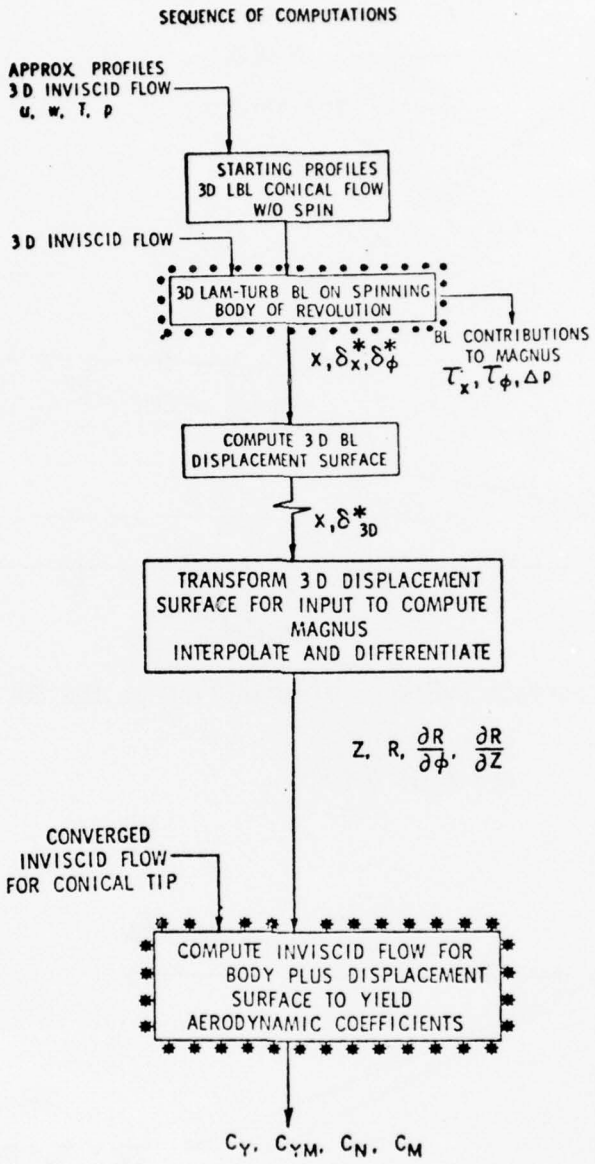

Figure 5. Sequence of Numerical Computations

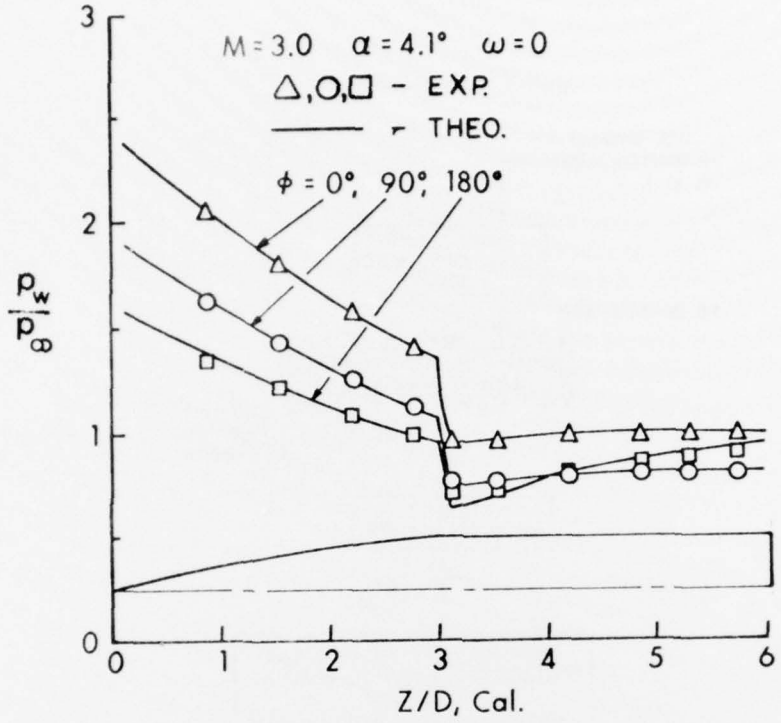

Figure 6. Surface Pressure Distribution on the SOC Model

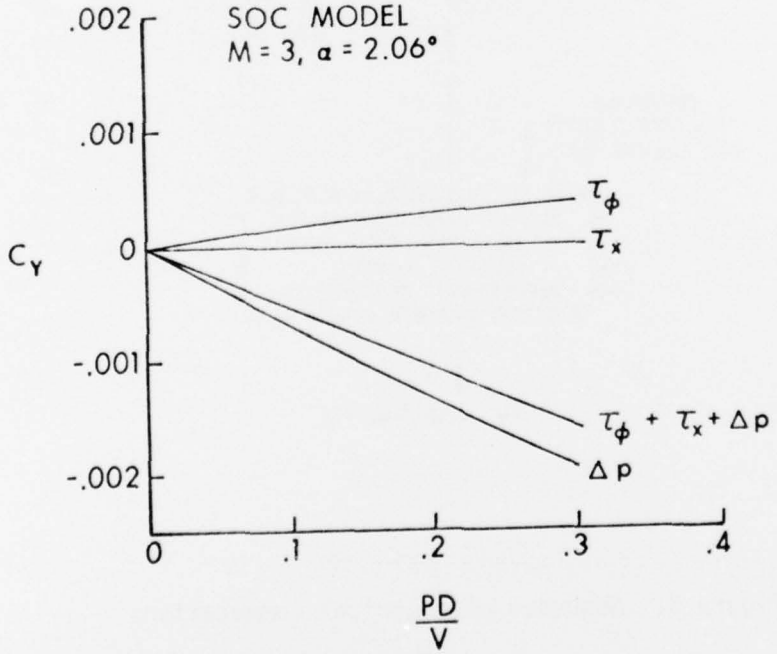

Figure 7. Turbulent Boundary Layer Contributions to Magnus Force

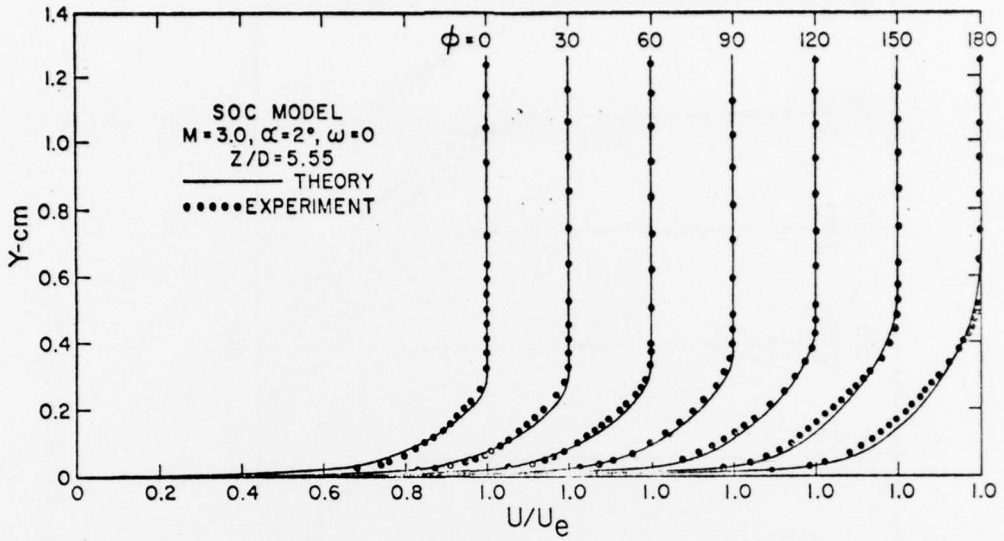

Figure 8. Velocity Profiles, Theory Compared With Experiment

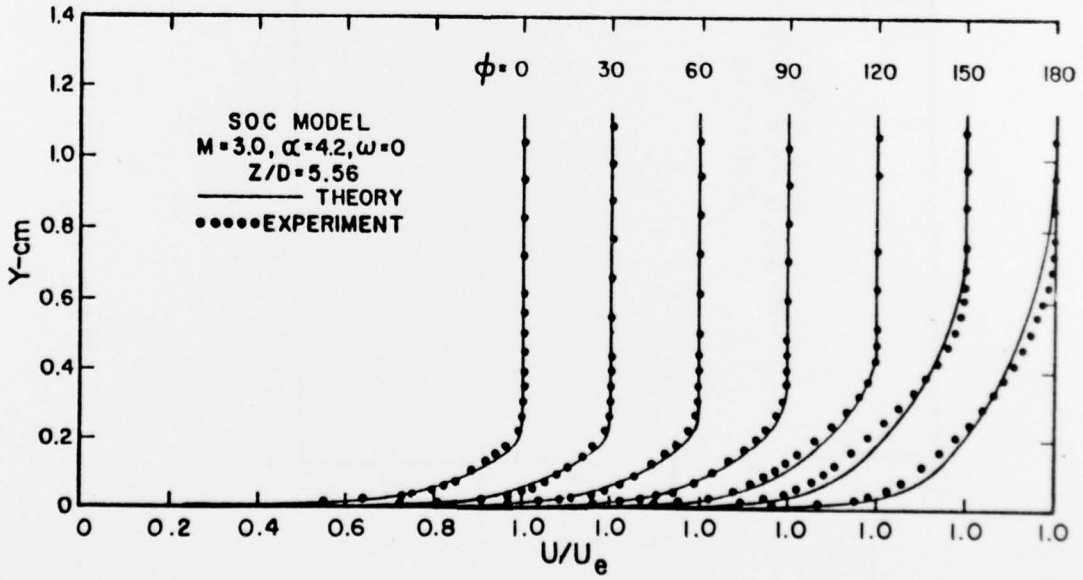

Figure 9. Velocity Profiles, Theory Compared With Experiment

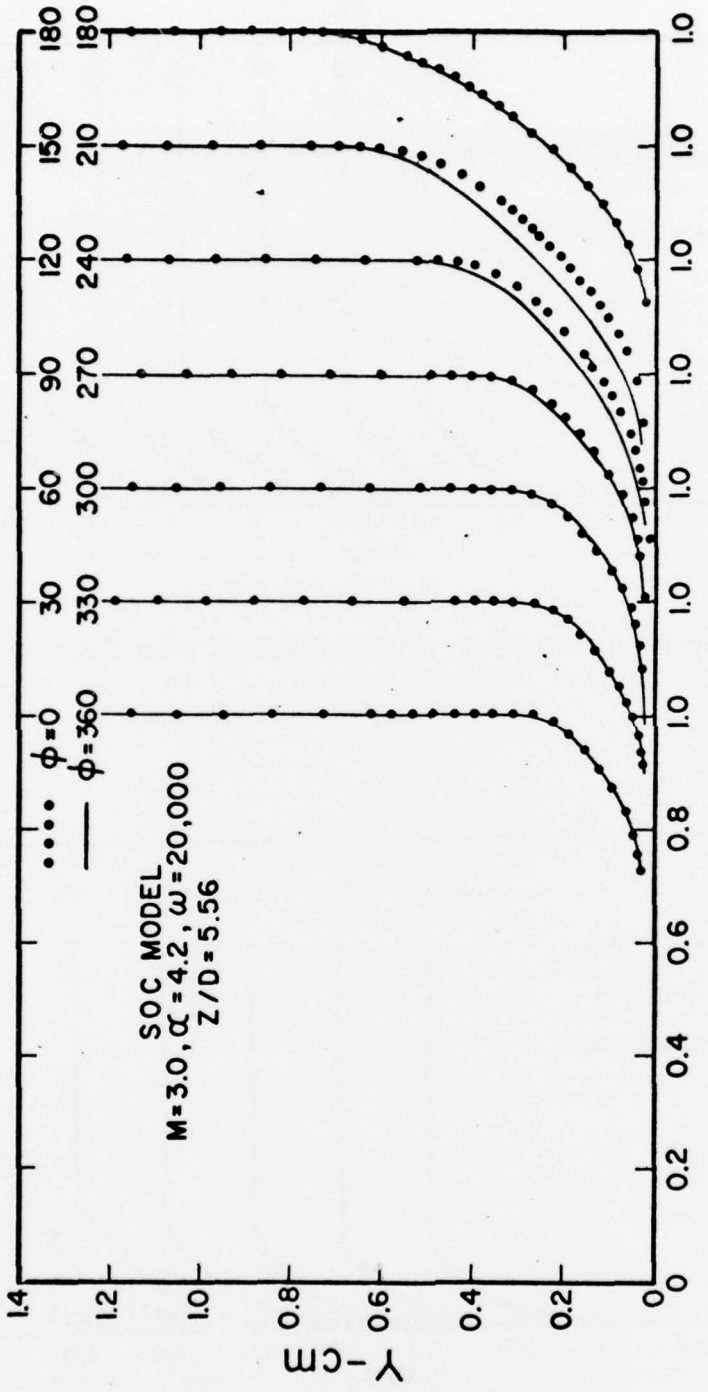

Figure 10. Experimental Velocity Profiles, Effects of Spin

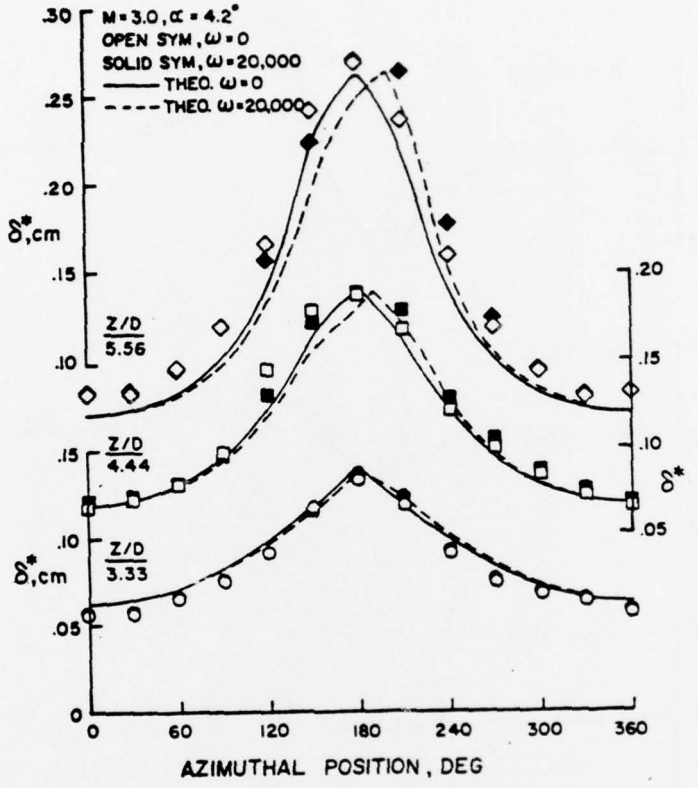

Figure 11. Boundary Layer Displacement Thickness, δ^*_x, Compared With Experiment, SOC Model

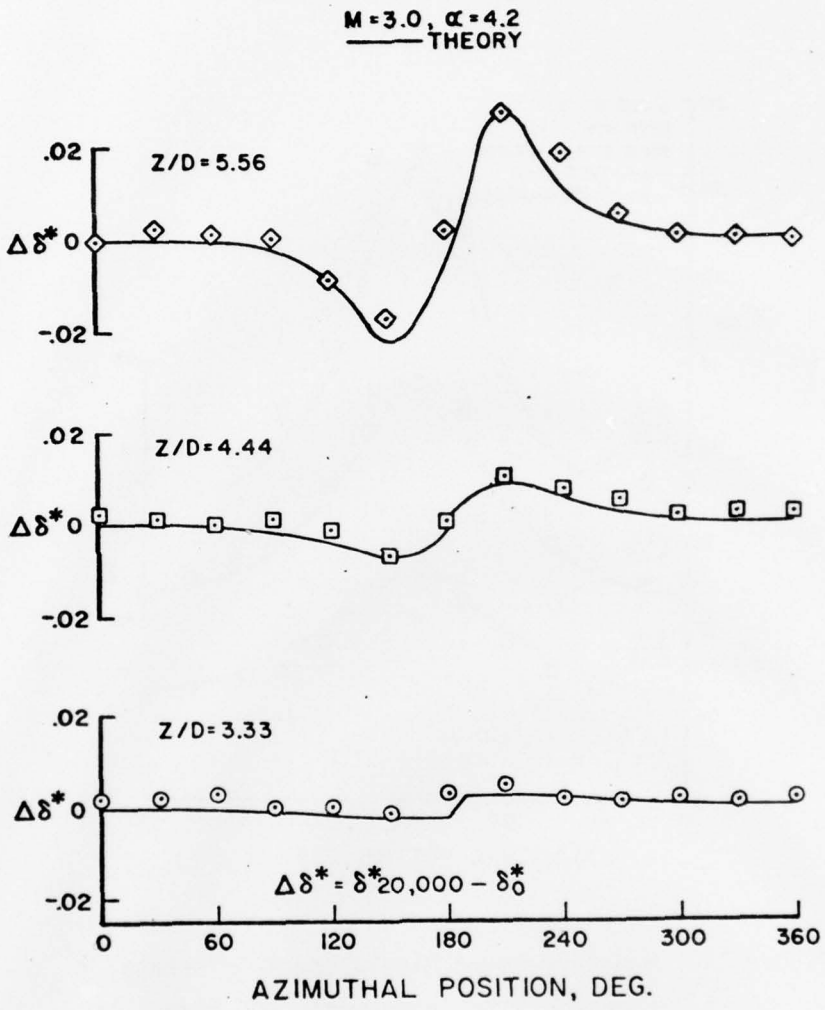

Figure 12. Increment of Displacement Thickness, $\Delta\delta^*_x$, Due to Spin, SOC Model

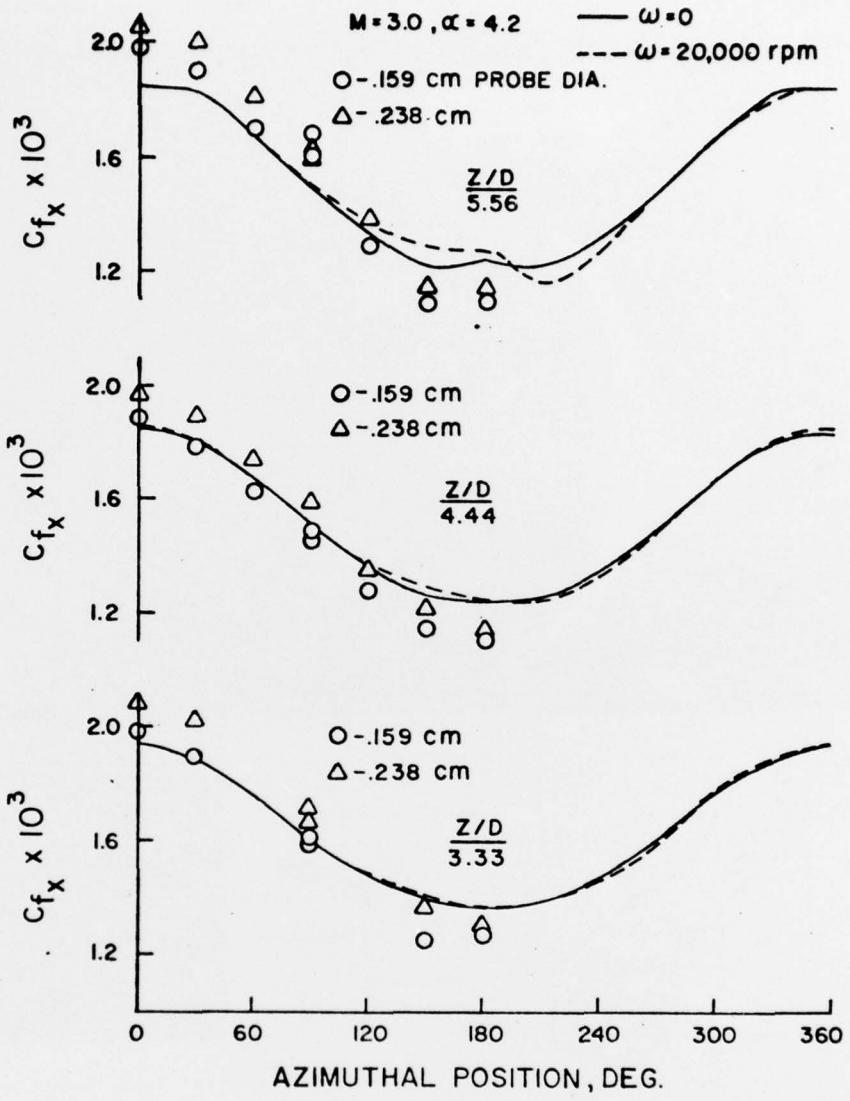

Figure 13. Preston Tube Skin Friction Results, SOC Model

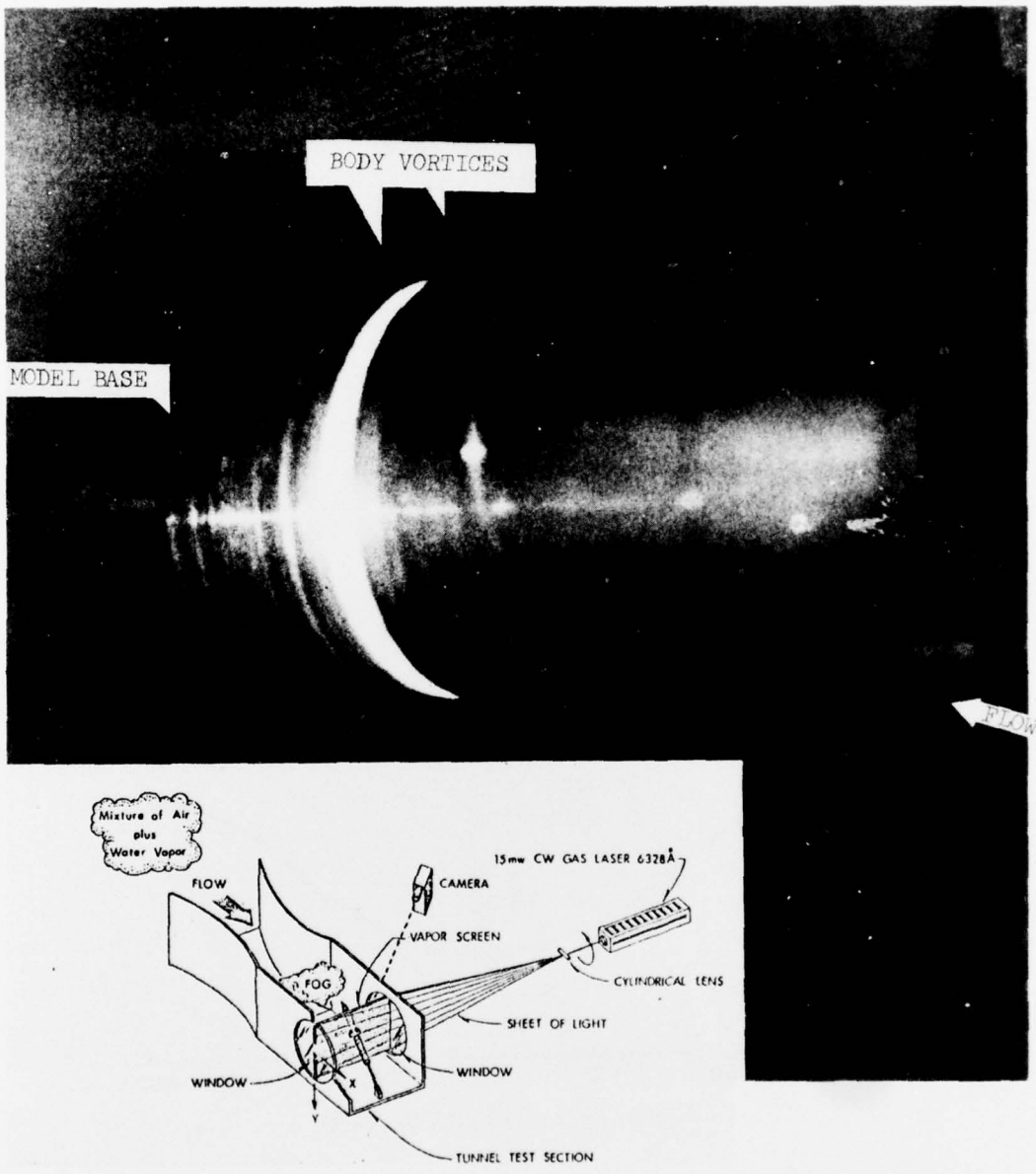

Figure 14. Vapor Screen Photograph, SOC Model, M = 3.0, α = 10°

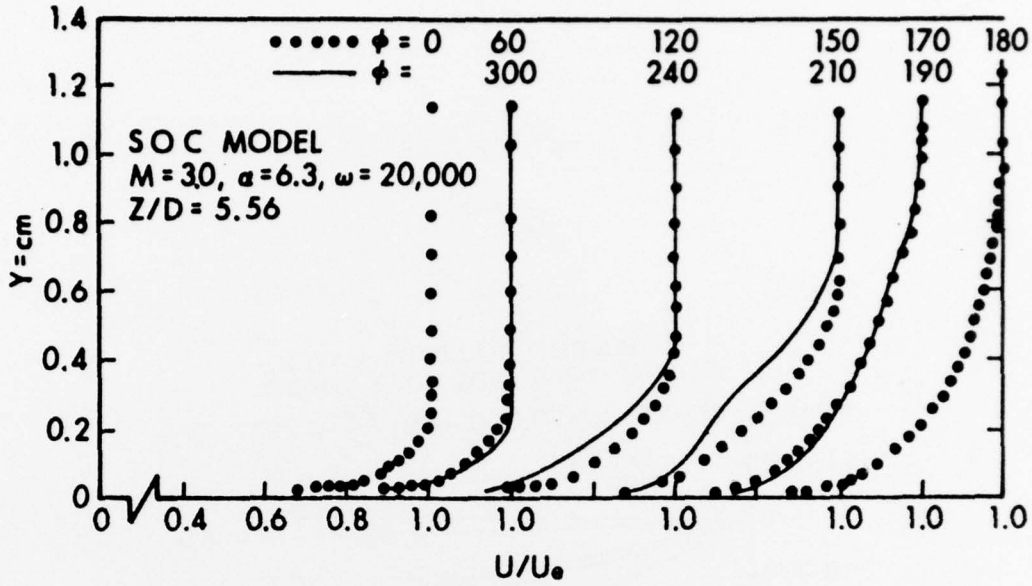

Figure 15. Experimental Velocity Profiles, Effects of Spin, $\alpha = 6.3°$

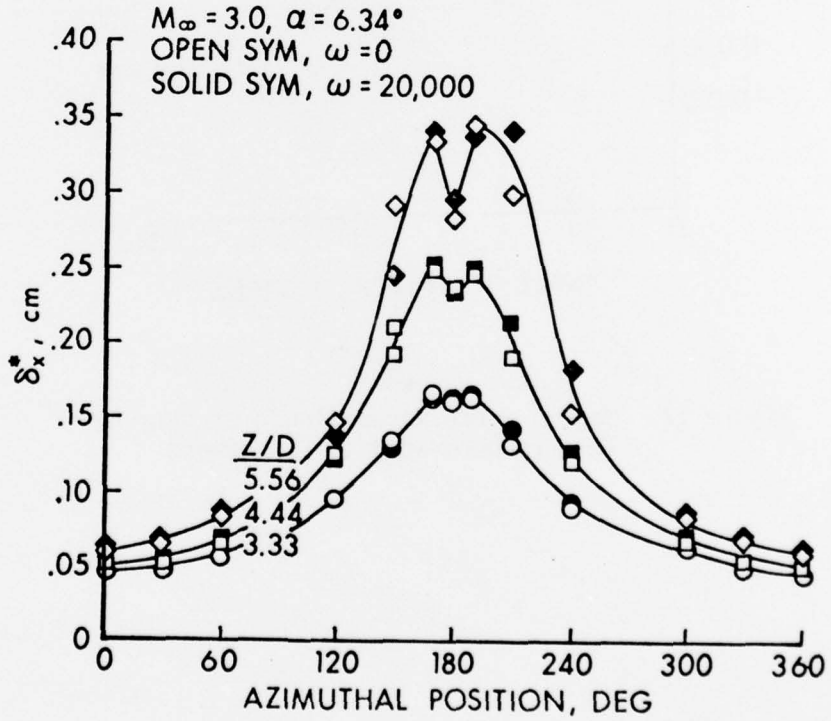

Figure 16. Experimental Boundary Layer Displacement Thickness, SOC Model, $\alpha = 6.3°$

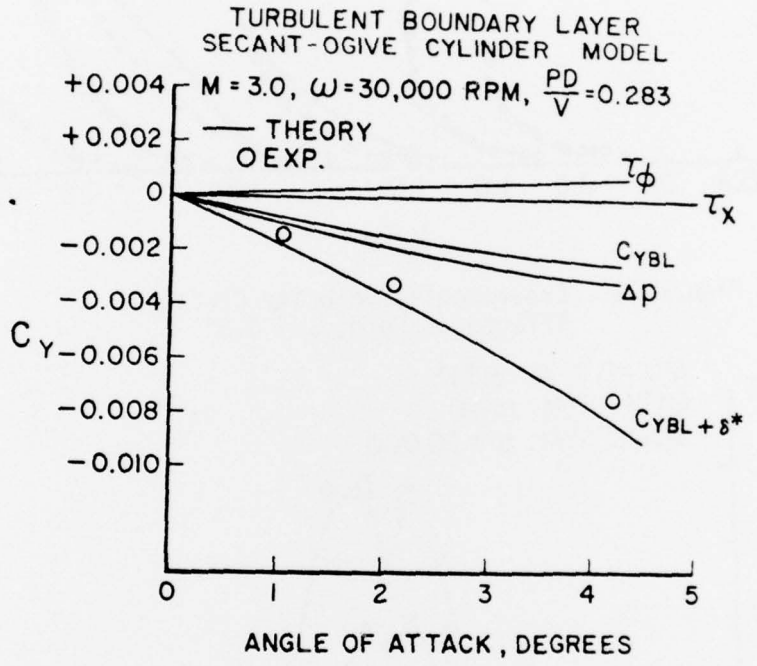

Figure 17. Magnus Force Versus Angle of Attack, Theory Compared With Experiment

LIST OF SYMBOLS

c_f	skin friction coefficient
c_p	specific heat at constant pressure
C_n	normal force coefficient
C_Y	Magnus (side) force coefficient
D	diameter of base of model
h	static enthalpy
k_t	turbulent conductivity
ℓ	mixing length
p	pressure
P	spin rate, radians per second
Pr_t	turbulent Prandtl number, $c_p \varepsilon / k_t$
r	local radius of model
Re_ℓ	Reynolds number based on model length
u,v,w	velocities in boundary layer coordinates
V	velocity along model trajectory
x	surface coordinate in longitudinal direction
y,Y	coordinate perpendicular to local surface
z	cylindrical coordinate along model axis
α	angle of attack
ε	turbulent eddy viscosity
δ	boundary layer thickness
δ^*	boundary layer displacement thickness

LIST OF SYMBOLS (Continued)

Δp	centrifugal pressure gradient contribution to side force
η	transformed y coordinate
μ	molecular viscosity
ξ	transformed x coordinate
ρ	density
τ_x	longitudinal velocity wall shear contribution to side force
τ_ϕ	circumferential velocity wall shear contribution to side force
ϕ	coordinate in circumferential (azimuthal) direction

Subscripts

e	edge of boundary layer
w	model wall conditions
x	quantity in x direction
∞	free stream reference condition
ϕ	quantity in azimuthal direction

Superscripts

$'$	fluctuating quantity
-	time averaged quantity

DISTRIBUTION LIST

No. of Copies	Organization
12	Commander Defense Documentation Center ATTN: DDC-TCA Cameron Station Alexandria, Virginia 22314
1	Commander US Army Materiel Development and Readiness Command ATTN: DRCDMA-ST 5001 Eisenhower Avenue Alexandria, Virginia 22333
1	Commander US Army Aviation Systems Command ATTN: DRSAV-E 12th and Spruce Streets St. Louis, Missouri 63166
1	Director US Army Air Mobility Research and Development Laboratory Ames Research Center Moffett Field, CA 94035
1	Commander US Army Electronics Command ATTN: DRSEL-RD Fort Monmouth, NJ 07703
1	Commander US Army Jefferson Proving Ground ATTN: STEJP-TD-D Madison, Indiana 47250
5	Commander US Army Missile Research and Development Command ATTN: DRDMI-X DRDMI-T DRDMI-TD Mr. R. Becht Mr. R. Deep Dr. D. Spring Redstone Arsenal, AL 35809
1	Commander US Army Tank Automotive Development Command ATTN: DRDTA-RWL Warren, Michigan 48090
2	Commander US Army Mobility Equipment Research and Development Command ATTN: Tech Docu Cen, Bldg 315 DRSME-RZT Fort Belvoir, Virginia 22060
1	Commander US Army Armament Materiel Readiness Command Rock Island, Illinois 61202
3	Commander US Army Armament Research and Development Command ATTN: DRDAR-LCA-F Mr. D. Mertz Mr. E. Falkowski Mr. A. Loeb Dover, New Jersey 07801

DISTRIBUTION LIST

No. of Copies	Organization
1	Commander US Army Harry Diamond Laboratories ATTN: DRXDO-TI 2800 Powder Mill Road Adelphi, Maryland 20783
1	Director US Army TRADOC Systems Analysis Activity ATTN: ATAA-SA White Sands Missile Range New Mexico 88002
1	Commander US Army Research Office P.O. Box 12211 Research Triangle Park North Carolina 27709
2	Commander David W. Taylor US Naval Ship Research and Development Center ATTN: Dr. S. de los Santos Mr. Stanley Gottlieb Bethesda, Maryland 20084
1	Commander US Naval Surface Weapons Center ATTN: Dr. T. Clare, Code DK20 Dahlgren, Virginia 22448
4	Commander US Naval Surface Weapons Center ATTN: Code 312, Mr. S. Hastings Code 313, Mr. R. Lee Mr. W. Yanta Mr. R. Voisinet Silver Spring, Maryland 20910
1	AEDC (Mr. J. Whitfield) Arnold AFS Tennessee 37389
2	Director NASA Langley Research Center ATTN: MS 185, Tech Library MS 161, Mr. D. Bushnell Langley Station Hampton, Virginia 23365
1	Douglas Aircraft Company McDonnell-Douglas Corp. ATTN: Dr. Tuncer Cebeci 3855 Lakewood Blvd. Long Beach, California 90801
1	Sandia Laboratories ATTN: Dr. F. G. Blottner P.O. Box 5800 Albuquerque, New Mexico 87115
2	Princeton University James Forrestal Research Center Gas Dynamics Laboratory ATTN: Prof. S. Bogdonoff Prof. I. Vas Princeton, New Jersey 08540
1	University of California Department of Mechanical Engineering ATTN: Prof. H. A. Dwyer Davis, California 95616
1	University of Delaware Mechanical and Aerospace Engineering Department ATTN: Dr. J. E. Danberg Newark, Delaware 19711

DISTRIBUTION LIST

No. of Copies	Organization
2	University of Virginia Department of Aerospace Engineering and Engineering Physics ATTN: Prof. I. Jacobson Prof. J. B. Morton Charlottesville, Virginia 22904
	Aberdeen Proving Ground
	Marine Corps Ln Ofc Director, USAMSAA